Crystal structural variation and phase transition in caesium trichlorocuprate at high pressure

1994 J. Phys.: Condens. Matter 6 3125

(http://iopscience.iop.org/0953-8984/6/17/005)

J. Phys.: Condens. Matter 6 (1994) 3125–3136. Printed in the UK

Crystal structural variation and phase transition in caesium trichlorocuprate at high pressure

Andrew G Christy†‡, Ross J Angel§‖, Julian Haines†¶ and Simon M Clark‡

† Department of Chemistry, University of Leicester, LE1 7RH, UK

‡ SERC Daresbury Laboratory, Warrington WA4 4AD, UK

§ Research School of Geological and Geophysical Sciences, University College London, Gower Street, London WC1E 6BT, UK

Received 21 January 1994

Abstract. Single-crystal and powder x-ray diffraction experiments, together with Raman spectroscopy, show that the 'hexagonal perovskite' $CsCuCl_3$ undergoes a phase transition at pressures between 1.65 and 3.1 GPa. The transition pressure is strongly dependent upon the form of the sample, being lower in powder specimens than in single crystals. The transition is first order in character and is accompanied by a 1.8% volume charge and a reduction in the length of the *c*-axis from the six-layer repeat of the room pressure phase to a two-layer repeat. These observations, together with the change in Raman modes at the transition lead us to conclude that the high-pressure structure contains statically disordered Jahn–Teller-distorted $CuCl_6$ octahedra, in contrast to the known high-temperature phase, which contains dynamically disordered distorted octahedra, and the low-pressure, ambient-temperature structure, which displays an ordered array of distorted octahedra.

1. Introduction

Many ABX_3 halides (A = K, Rb Cs, Tl; B = Mg, V, . . ., Cu: X = Cl, Br, I) crystallize in the 'hexagonal perovskite' structure. Infrared and structural data for a large number of them are reported by McPherson and Chang (1973). The structure can be described as a hexagonal array of face-sharing BX_6 octahedra cross linked by A atoms. The A and X atoms together form a hexagonal close-packed sublattice, which may be compared with the corresponding cubic close-packed AX_3 array in the more widely known 'cubic perovskite' topology of compounds such as $CaTiO_3$. The two structure types are in fact polytypically related with $2H$ and $3C$ layer stacking patterns in the notation of Ramsdell (1947). Under ambient conditions $CsMnCl_3$ has an intermediate $9H$ structure, which transforms via a $6H$ structure to the $3C$ polytype with increasing pressure. $RbMnCl_3$ and several related fluorides also transform from the $6H$ structure at ambient to the $3C$ phase at pressure (Longo and Kafalas 1971). By contrast, $CsCdBr_3$ retains the $2H$ structure from room pressure to over 20 GPa (Léger *et al* 1990).

Another type of structural variation seen in the hexagonal perovskites is the adoption of ordered superstructures when the BX_6 coordination octahedron is distorted due to the Jahn–Teller effect. This is likely if the B atom is a d^4 or d^9 species (Cr^{2+} or Cu^{2+}). The compounds $RbCuCl_3$, $RbCrCl_3$ and $CsCrCl_3$ all possess the aristotypic hexagonal perovskite

‖ Current address: Bayerisches Geoinstitut, Universität Bayreuth, D95440 Bayreuth, Germany.

¶ Current address: CNRS Laboratoire de Physico-Chimie des Materiaux, 1 Place Aristide Briand, 92190 Meudon, France.

0953-8984/94/173125+12$19.50

structure at high temperature but transform to lower-symmetry ordered superstructures under cooler conditions. The behaviour of these compounds is reviewed in detail by Tanaka *et al* (1986a). The Jahn–Teller energy is large enough for the octahedra to be distorted at all temperatures but the distortion is orientationally disordered in the high-temperature phases. Tanaka *et al* (1986a, b) describe the phase transitions in terms of the onset of long-range order within face-sharing octahedral chains together with a pseudospin interaction between neighbouring chains. The two ordering processes may or may not be coupled and different ordered states may be favoured, leading to distinctive transition behaviour for each of the compounds.

$CsCuCl_3$ is unique among these compounds in that its room-temperature structure is hexagonal with a tripled c-axis with the long Cl–Cu–Cl bonds helically distributed about screw hexad axes in the enantiomorphic space groups $P6_122$ or $P6_522$ (Wells 1947, Schlueter *et al* 1965). At present this appears to be the only phase in which a helical displacement pattern of atoms away from their ideal positions has been observed. The transformation to the disordered structure occurs at 423 K, 1 bar (Kroese *et al* 1971). The transition is discontinuous as required by the symmetry criteria of Birman (1966) since it occurs at the $0, 0, \frac{1}{3}$ point in the Brillouin zone of the high-temperature (HT) phase. The order parameter associated with the displacement is four dimensional and a basis set can be constructed from sine and cosine components of right- and left-circular helical modulations (Hirotsu 1977). Raman and far-infrared studies (Akiyama *et al* 1979, Petzelt *et al* 1981) located very-low-frequency modes in the low-temperature phase whose symmetry is consistent with their being fluctuations in amplitude, phase and chirality of the modulation. The symmetry species are respectively $A_1 + A_2 + E_2$ corresponding to Δ_6 in the HT phase (notation of Koster *et al* 1963, equivalent to τ_5 ($k = 0, 0, 2\pi/3c$) in the notation of Kovalev 1964). The transformation has been characterized in detail by optical rotation, birefringence and x-ray diffraction (Hirotsu 1975) and by elastic, quasielastic and inelastic neutron scattering (Graf *et al* 1986, 1989).

The amplitude of the primary order parameter in the modulated phase is proportional to the offset of the Cu atoms from the screw hexad axis. Structure refinements may therefore be used to follow the temperature and pressure evolution of Q and to quantify the terms in the Landau free-energy expansion. Hirotsu (1977) presents a detailed analysis of the HT behaviour. A Landau theoretical treatment of the transition has also been provided by Kroese and Maaskant (1974). $CsCuCl_3$ was selected for examination at high pressure in this study because it is a simple example of a compound in which a phase transition results from ordering of Jahn–Teller distorted octahedra and further transitions were thought to be likely at pressure. The behaviour of related compounds suggested that change in the polytypic stacking of the pseudo-close-packed $CsCl_3$ layers was also a possibility.

2. Experimental details

2.1. Sample preparation

$CsCuCl_3$ was prepared from an aqueous solution of CsCl and $CuCl_2.2H_2O$ as red-brown needles up to 2 mm long. Some yellow plates of Cs_2CuCl_4 were intergrown since an excess of Cu was not used (Akiyama *et al* 1979). However, mechanical separation of the phases was straightforward. Separated single crystals were studied by x-ray diffraction or were gently ground to powder and examined by Raman spectroscopy and energy-dispersive powder x-ray diffraction.

Table 1. Axial and bulk compression from single-crystal diffraction. Room pressure cell parameters: a = 7.218(2) Å, c = 18.183(2) Å, V = 820.4(5) Å^3.

P (GPa)	a/a_0	c/c_0	V/V_0
0.00	1.0000	1.0000	1.0000
0.12	0.9969(3)	0.9982(1)	0.9920(6)
0.34	0.9925(1)	0.9950(1)	0.9801(3)
0.64	0.9870(3)	0.9907(1)	0.9649(6)
0.82	0.9832(3)	0.9876(1)	0.9548(6)
1.01	0.9810(1)	0.9865(1)	0.9496(3)
1.33	0.9754(3)	0.9819(1)	0.9342(6)
1.68	0.9710(3)	0.9782(1)	0.9222(6)
1.77	0.9693(3)	0.9767(1)	0.9176(6)
2.07	0.9657(2)	0.9738(1)	0.9083(3)
2.44	0.9612(3)	0.9700(1)	0.8961(6)
2.48	0.9612(3)	0.9700(1)	0.8963(6)
2.79	0.9572(2)	0.9669(1)	0.8860(3)
3.04	0.9558(3)	0.9650(1)	0.8818(7)

Table 2. Unit-cell parameters from powder diffraction. The c parameter of the *sub-cell* is reported for the low-pressure phase: the true cell repeat is 3c. The first set data listed were collected with nujol as the pressure medium, the second set with petroleum ether.

P (GPa)	a (Å)	c (Å)	V (Å^3)
0.00	7.213(2)	6.058(6)	273.0(3)
0.23	7.116(4)	6.013(10)	263.7(5)
0.82	7.083(3)	5.976(7)	259.6(3)
1.09	7.032(5)	5.969(10)	255.6(6)
1.27	7.042(3)	5.970(8)	256.4(4)
1.78	6.951(4)	5.967(11)	249.7(5)
2.34	6.853(33)	5.911(86)	240.4(4)
2.46	6.847(33)	5.903(84)	239.7(4.1)
2.73	6.838(37)	5.890(94)	238.5(4.6)
3.02	6.819(38)	5.876(98)	236.6(4.7)
3.53	6.774(36)	5.859(92)	232.8(4.4)
4.37	6.711(35)	5.827(91)	227.3(4.3)
5.39	6.711(35)	5.795(90)	226.0(4.2)
6.49	6.662(29)	5.765(74)	221.6(3.4)
0.00	7.221(5)	6.034(11)	272.5(6)
0.75	7.108(3)	6.002(8)	262.5(4)
1.52	7.011(13)	5.996(32)	255.2(1.7)
1.80	6.957(12)	5.941(29)	249.0(1.5)
2.09	6.929(2)	5.963(6)	247.9(3)
2.28	6.876(27)	5.923(68)	242.5(3.4)
2.67	6.846(34)	5.902(86)	239.6(4.2)
3.26	6.813(32)	5.870(82)	236.0(4.0)
3.75	6.795(30)	5.845(77)	233.7(3.7)
5.15	6.771(13)	5.806(33)	230.5(1.6)

2.2. *Single-crystal diffraction*

$CsCuCl_3$ crystals of less than 100 μm maximum linear dimension were mounted in a modified Merrill–Bassett diamond cell. The chloride was found to dissolve in the conventional methanol–ethanol pressure medium at elevated pressure so a low-boiling-point fraction of petroleum ether was used as the pressure medium. The pressure was measured by ruby fluorescence using the calibration of Mao *et al* (1986). The precision of the pressure measurement was ±0.03 GPa (Angel *et al* 1992). No significant broadening of the R_1 and

R_2 peaks was observed nor was any increase in their separation. The pressure medium was therefore inferred to remain essentially hydrostatic over the 0–5 GPa pressure range. X-ray diffraction measurements were carried out on a Picker four-circle diffractometer equipped with a conventional Mo x-ray source (λ Kα = 0.7093 Å). Cell parameters at pressure (table 1) were determined from the positions of 17 reflections with $13° < 2\theta < 26°$ centred by the method of King and Finger (1979) to eliminate the effects of crystal offsets and diffractometer aberrations. Intensity data out to 60° 2θ were collected with Nb-filtered radiation and constant-precision step scans, each of which was inspected manually and integrated with a modified Lehmann–Larsen algorithm to set the backgrounds. The resulting intensities were corrected for absorption by the crystal and diamond-anvil cell and for shadowing by the gasket and were reduced to structure factors, which were averaged in point group 6/*mmm*. Structure refinements were carried out with RFINE90, a development version of RFINE4 (Finger and Prince 1975) with neutral atom form factors taken from the *International Tables for X-ray Crystallography* (1992). Final refinement indices are given in table 3, refined parameters in table 4, and bond lengths and angles in tables 5 and 6.

Table 3. Data collection and refinement details—single-crystal diffraction.

	0.00 GPa	0.12 GPa	0.82 GPa	1.68 GPa	2.44 GPa	2.79 GPa
N_{obs}	162	173	122	159	167	173
$R_{int} F > 6\sigma_F$	0.039	0.030	0.022	0.037	0.030	0.041
R_w	0.056	0.046	0.043	0.039	0.037	0.048
R_u	0.078	0.067	0.047	0.058	0.051	0.062
G_{fit}	1.88	1.78	1.19	1.48	1.40	1.54

Table 4. Refined structural parameters—single-crystal diffraction. Cs and Cl1 on special positions x, $2x$, $\frac{1}{4}$; Cu on special position x, 0, 0.

	0.00 GPa	0.12 GPa	0.82 GPa	1.68 GPa	2.44 GPa	2.79 GPa
Cs: x	0.3550(3)	0.3546(2)	0.3538(3)	0.3527(2)	0.3516(2)	0.3514(3)
Cs: B_{iso}	2.5(1)	1.95(7)	1.91(8)	1.83(5)	1.96(4)	1.34(7)
Cu: x	0.0644(9)	0.0633(7)	0.0566(11)	0.0531(7)	0.0508(6)	0.0528(9)
Cu: B_{iso}	1.7(2)	1.4(1)	1.6(2)	1.7(1)	1.64(7)	1.4(1)
Cl1: x	0.8896(12)	0.8875(10)	0.8821(13)	0.8807(10)	0.8743(7)	0.8760(12)
Cl1: B_{iso}	1.4(3)	2.0(2)	2.1(3)	2.3(2)	1.9(2)	2.2(3)
Cl1: x	0.3576(21)	0.3597(16)	0.3559(19)	0.3576(13)	0.3583(11)	0.3580(18)
Cl1: y	0.2119(16)	0.2117(4)	0.2078(17)	0.2046(17)	0.2032(9)	0.2039(13)
Cl1: z	0.2424(8)	0.2396(4)	0.2405(5)	0.2420(4)	0.2427(3)	0.2430(6)
Cl1: B_{iso}	2.6(3)	1.6(2)	1.8(2)	1.5(1)	1.7(1)	1.0(2)

2.3. Raman spectroscopy

The sample was loaded into a Diacell diamond anvil cell with ruby chips for pressure calibration and nujol as the quasi-hydrostatic pressure medium. A stainless steel gasket was used, about 450 μm thick with a sample hole 250 μm in diameter. Data were collected on a Coderg T-800 spectrometer using the 647.1 nm line of a Spectra Physics model 164 Kr^+ laser. Peak positions were measured manually; their zero-pressure positions and pressure dependences are given in table 7. The precision of the measurement of peak position is estimated as ± 2 cm^{-1}.

Table 5. $CuCl_6$ octahedron—bond lengths and angles. QE is the quadratic elongation of the octahedron and AV its angle variance, both defined by Robinson *et al* (1971). The Cu offset is the distance of the Cu position x, 0, 0 from the unit-cell origin. Cu–Cu is the distance between consecutive Cu atoms along a face-sharing octahedral chain.

	0.00 GPa	0.12 GPa	0.82 GPa	1.68 GPa	2.44 GPa	2.79 GPa
Cu–Cl2 (Å)	2.789(13)	2.823(9)	2.756(10)	2.718(8)	2.687(6)	2.673(10)
Cu–Cl1 (Å)	2.351(3)	2.359(3)	2.347(4)	2.317(3)	2.343(3)	2.328(2)
Cu–Cl1 (Å)	2.292(15)	2.272(10)	2.268(11)	2.282(8)	2.283(6)	2.267(11)
⟨Cu–Cl⟩ (Å)	2.478	2.488	2.457	2.439	2.438	2.423
Volume (Å^3)	19.74	19.87	19.31	18.94	18.99	18.62
QE	1.0261	1.0291	1.0237	1.0210	1.0169	1.0176
AAV	36.03	36.13	30.92	28.21	22.33	24.17
Cu offset (Å)	0.465(7)	0.456(5)	0.405(7)	0.372(5)	0.353(4)	0.365(6)
Cu–Cu (Å)	3.066(1)	3.059(1)	3.020(1)	2.988(1)	2.961(1)	2.953(1)

Table 6. $CsCl_{12}$ dodecahedron—bond lengths and angles.

	0.00 GPa	0.12 GPa	0.82 GPa	1.68 GPa	2.44 GPa	2.79 GPa
Cs–Cl1	4.034(9)	4.009(3)	3.920(9)	3.871(7)	3.790(5)	3.790(9)
Cs–Cl1	3.643(14)	3.674(8)	3.632(11)	3.571(8)	3.529(6)	3.513(11)
Cs–Cl1	3.644(14)	3.603(9)	3.558(11)	3.528(8)	3.597(6)	3.488(10)
Cs–Cl2	3.606(12)	3.621(7)	3.561(11)	3.530(8)	3.494(6)	3.472(8)
Cs–Cul1	3.635(9)	3.583(8)	3.566(9)	3.521(7)	3.489(5)	3.467(9)
Cs–Cul1	3.617(12)	3.603(9)	3.547(12)	3.484(8)	3.449(6)	3.442(8)
⟨Cs–Cl⟩	3.696	3.682	3.631	3.584	3.540	3.529
Volume	119.4	118.4	113.4	109.3	105.4	104.3

Table 7. Raman modes of $CsCuCl_3$ at high pressure. The column headed 'ν_0 (cm^{-1}) (HT)' gives the frequencies reported by Petzelt *et al* (1981) for the HT phase at 398 K. The parameters ν_0 and $\delta\nu/\delta P$ are the estimated Raman frequencies at room pressure and their pressure dependence derived from a linear fit of frequency with pressure.

ν_{obs} (cm^{-1})	ν_0 (cm^{-1})	ν_0 (cm^{-1}) (HT)	$\delta\nu/\delta P$ (cm^{-1} GPa^{-1})	Assignment
Low-pressure phase (ν_{obs} at ambient pressure)				
287	285.9(6)		4.5(3)	E_1, A_1
264	264.6(2.6)		4.8(1.5)	A_1
192	188.5(1.6)		4.7(8)	E_2
188	187.6(—)		6.4(—)	E_1
178	176.9(9)		5.9(6)	E_1, A_1
161	160.3(—)		8.7(—)	E_1
154	155.1(3.1)		8.1(1.6)	E_2
102	101.6(2.6)		8.9(1.8)	E_1, A_1
High-pressure phase (ν_{obs} at 2.9 GPa)				
290	277.4(1.1)	286, 285	4.5(6)	A_{1g}, E_{1g}
203	192.0(7)	188, 192	3.4(1.2)	E_{1g}, E_{2g}
195	158.5(1.5)	155	11.8(1.9)	E_{2g}

2.4. Powder diffraction

Evidence of a phase transition was seen in both single-crystal x-ray and Raman studies. Since single crystals were found to fragment after cycling through the transition structural studies of the high-pressure phase were precluded. Therefore energy-dispersive powder diffraction was used to investigate the behaviour of $CsCuCl_3$ above and below the transition.

The chloride was ground with NaCl as an internal pressure calibrant and loaded into a Diacell diamond-anvil cell. Pre-indented inconel gaskets with samples holes ~200 μm in diameter were used. Separate runs were conducted with both nujol and petroleum ether as pressure media in order to allow direct comparison with the single-crystal x-ray and Raman studies, and to establish whether the choice of medium had any effect on sample behaviour. Data were collected on Station 9.7 at the Daresbury Synchrotron Radiation Source. A diffraction angle 2θ of about 5° (refined as 4.777° using a Si standard) was chosen so as to minimize interference between Cs fluorescence and important Bragg peaks. Peak positions were fitted to Gaussian functions using the NGAUS macro on the Station microVAX. Seven strong reflections (100, 103, 110, 006, 203, 106, 206) were used to refine cell parameters, which are reported in table 2.

3. Results

3.1. Single-crystal diffraction

The unit-cell parameters of $CsCuCl_3$ were determined at 14 pressures from ambient pressure to 3.04 GPa (table 1), and the bulk compression is displayed in figure 1. There was no deviation from hexagonal symmetry, and the presence of diffraction maxima at $l \neq 3n$ positions indicated that the structure remains in the low-pressure $P6_122$ phase over this pressure range. Upon compression to pressures in excess of 3.1 GPa the $l = 3n$ diffraction peaks became significantly broadened, the $l \neq 3n$ peaks became unobservable, and optically the crystal became opaque. This broadening appears to increase with increasing pressure. As the peaks could not be centred on the diffractometer, no estimate of the unit-cell parameters of the high-pressure could be made. Subsequent pressure reduction to 2.6 GPa resulted in the crystal becoming optically clear, the $l \neq 3n$ peaks reappearing, and the $l = 3n$ peaks becoming sharper, all of which indicate that the transition is, in principle, reversible. However, this recovery in intensity was not complete, suggesting that some irreversible damage of the crystal (possibly plastic deformation or creation of sub-grains) was induced by cycling through the phase transition.

The parameters of various equations of state (EOSs) for the low-pressure $P6_122$ phase were determined by least-squares fits to the volume–pressure data. The refined parameters of a Murnaghan EOS are $K = 15.9(7)$ GPa, $K' = 6.0(5)$, and those of a third-order Birch–Murnaghan finite-strain EOS are $K = 15.6(8)$, $K' = 6.8(7)$. The value of K'' in a fourth-order Birch–Murnaghan EOS refined to less than its ESD, and is therefore considered insignificant. The overall compression of the structure is anisotropic, with directions in the a–b-plane being approximately 50% more compressible (i.e. softer) than the c-axis: Murnaghan fits to the axial compressions yield $K = 42.7(1.9)$ GPa, $K' = 18.1(1.4)$ for the a-axis, and $K = 61.8(2.2)$, $K' = 16.6(1.6)$ for the c-axis.

The bulk compression of the structure appears to be accommodated equally between the $CuCl_6$ octahedra and the $CsCl_{12}$ dodecahedra; their bulk moduli calculated from the variation of their polyhedral volumes at pressure are 15.2(1.5) GPa and 15.1(1.6) GPa respectively for a third-order EOS. The compression of the $CuCl_6$ octahedra has two important internal features. The room-pressure Jahn–Teller distortion decreases with the application of pressure as a result of the two longer Cu–Cl2 bonds in each octahedron being significantly compressible while the four shorter bonds are essentially incompressible (table 5). Increasing pressure also results in a decrease of the offset of the Cu cation from the position 0, 0, 0 which it would occupy in a high-symmetry, $P6_3/mmc$ structure (figure 2). It should be noted that this decrease, which is the primary order parameter for

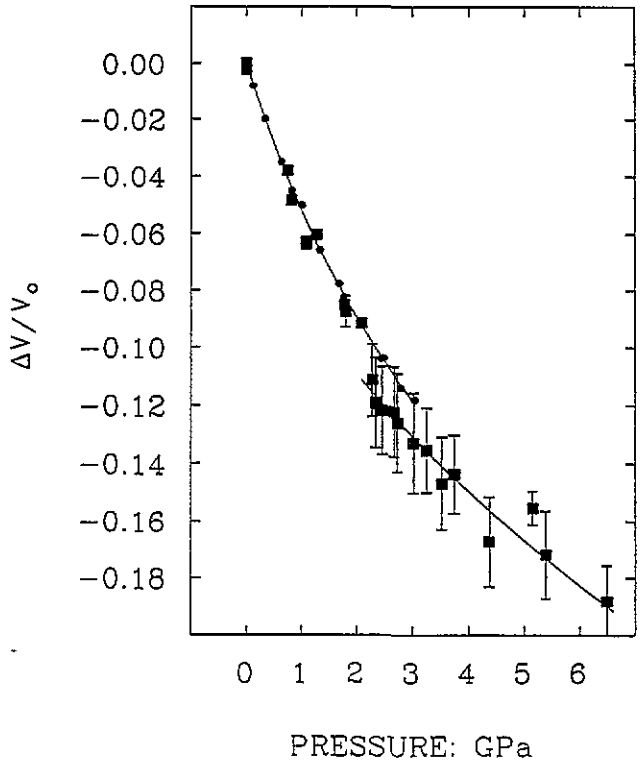

Figure 1. The variation of $\Delta V/V_0$ of $CsCuCl_3$ with pressure. Small symbols are data from the single-crystal diffraction experiments, for which the ESDs are smaller than the symbol size. Square symbols with error bars (1σ) are data from the powder-diffraction study. The lines are the Birch–Murnaghan EOSS for the low-pressure phase (single-crystal data) and the high-pressure phase (powder data), the parameters of which are given in the text.

the $P6_3/mmc \rightarrow P6_122$ phase transition, does not tend towards zero but retains a large finite value at the phase transition above 3.04 GPa.

The anisotropy of the structure as a whole does not arise from either this differential compression of the longer Cu–Cl bonds (as they are inclined to both the *a*- and the *c*-axis), nor from the internal distortion of the $CuCl_6$ octahedron; the changes in Cl–Cu–Cl bonds would in fact be expected to stiffen the (001) planes with respect to *c*. Similarly, the compression of the $CsCl_{12}$ polyhedron is isotropic, with all of the Cs–Cl bonds being compressed to 95±1% of their room-pressure values by 2.79 GPa. Two factors then remain to contribute to the observed anisotropy in the unit-cell compression. First, the Cu–Cu distance across the shared octahedral faces decreases at the same rate with pressure as the *c*-axis itself, suggesting the presence of significant Cu–Cu repulsion. Second, examination of the behaviour upon compression of the Cl–Cl distances within the structure (figure 3) reveals that the two of the eight symmetry-independent contacts are more compressible by a factor of approximately two than the remainder. These two compressible Cl–Cl contacts are oriented parallel to the (001) plane, and thus soften the *a*-axis relative to the *c*-axis. The reason for their relative compressibility lies within the topology of the structure; they are the only two of the eight Cl–Cl contacts that do *not* form edges of the $CuCl_6$ octahedra.

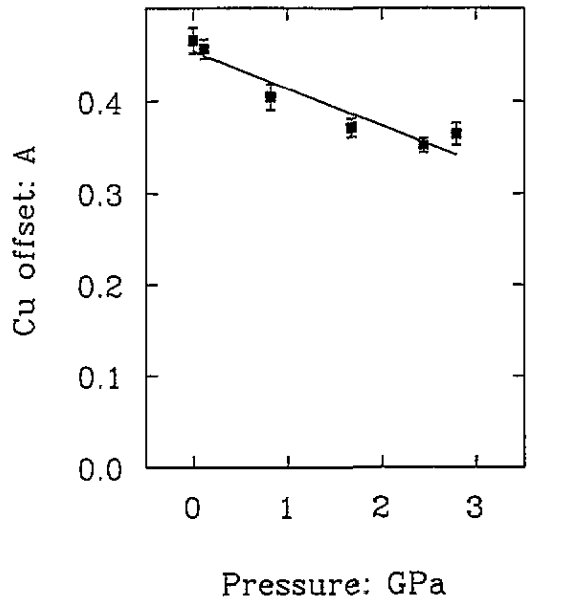

Figure 2. The offset of the Cu atom from the symmetry point 0, 0, 0 in the low-pressure phase, as determined by single-crystal diffraction. Note that it does *not* approach zero at the transition to the high-pressure phase.

3.2. Raman spectroscopy

Raman peaks below ~100 cm^{-1} were not measurable due to extremely strong Rayleigh scattering from the sample. According to the factor group analysis of Petzelt *et al* (1981) the full set of Raman-active modes in the low-pressure phase should be $\Gamma_{Raman} = 6A_1 + 14E_1 + 15E_2$. In practice they did not observe $1A_1$, $2A_2$ and $5E_2$ due to either weakness of scattering or overlap with other modes. Additionally, $1A_1 + 3E_1 + 6E_2$ modes were found to lie below 100 cm^{-1}. Above this frequency we located all the modes observed by Petzelt *et al* (1981) except for the E_2 mode near 132 cm^{-1}. Three $A_1 + E_1$ pairs were not resolved in our spectra, however (figure 4). In the pressure range 1.65–2.1 GPa the peaks corresponding to non-zone-centre modes of the subcell weakened and then disappeared, implying loss of the 3*c* modulation. In the same pressure interval three new modes appeared (figures 4 and 5; table 7) at frequencies consistent with their assignment as $1A_{1g} + 1E_{1g} + 1E_{2g}$ of a disordered phase similar to that observed at high temperature (Petzelt *et al* 1981). The remaining E_{2g} mode of the HT spectra was not observed, but it may be superimposed upon the observed E_{1g} mode.

3.3. Powder diffraction

There is an apparent discrepancy between the single-crystal x-ray data and the Raman data in that no phase transition was observed in the single-crystal until 3.0 GPa, whereas the Raman data imply the presence of a phase transition at just over 1.65 GPa. It was thought at first that this difference was caused by differing degrees of hydrostaticity in the pressure media (petroleum ether for the single-crystal study, nujol for the Raman work). However, powder x-ray datasets collected using both these pressure media were consistent with one another and showed that the choice of pressure medium had little effect on the transition behaviour, with both showing a reversible first-order phase transition at 2.10 ± 0.1 GPa.

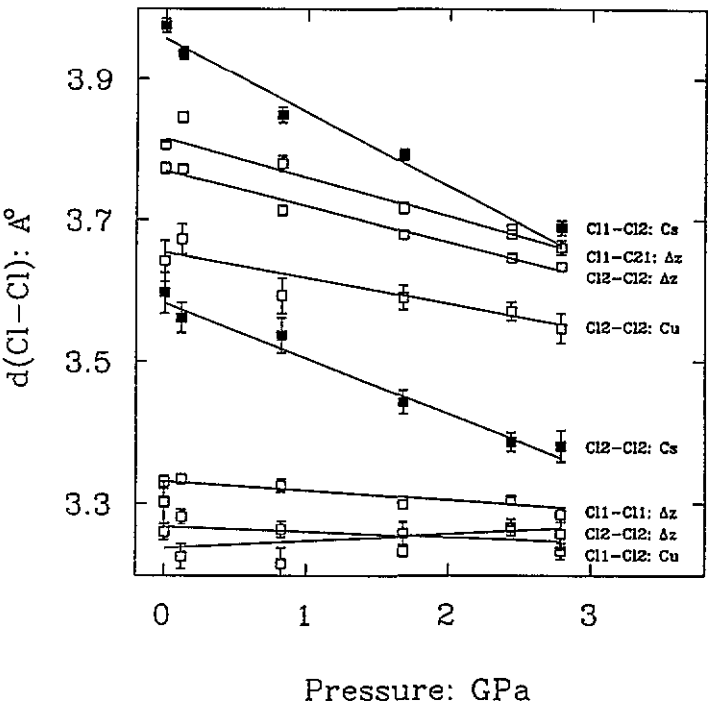

Figure 3. The variation with pressure of the length of Cl–Cl contacts in the low-pressure phase. Note that the two contacts labelled 'Cs' are significantly more compressible than all of the others. These two are oriented parallel to the (001) plane and therefore contribute to the greater compressibility of the directions in this plane compared to the stiffer *c*-direction.

No two-phase intergrowth of hysteresis was noted, in contrast to the Raman data, but this may be a consequence of the poor resolution of the EDS technique, combined with peak broadening in the diffraction pattern of the high-pressure phase.

The EOS determined from the cell parameter variation with pressure of the low-pressure phase (table 2) was found to be in agreement with the single-crystal data, but are of lower precision. Above the phase transition the diffraction peaks shift to higher energies (smaller *d*-spacings) and become broader (typically 0.9–1.3 keV rather than 0.6 keV) but may still be indexed upon a hexagonal unit cell. This broadening results in significantly greater ESDs for the cell parameters of the high-pressure phase (compare a = 7.213(2) Å, $c/3$ = 6.058(6) Å at 0 GPa with a = 6.876(27) Å, c = 5.923(68) Å at 2.28 GPa) and may indicate a small degree of peak splitting and fine-scale twinning, or the presence of residual strain. The bulk modulus for a Birch–Murnaghan third-order EOS of the high-pressure phase is 31.8(3.5) GPa if K' is constrained to be four; unconstrained refinements did not converge. From the EOSs we estimate the volume change at the transition pressure of 2.1 GPa to be ~4.5 $Å^3$ per $c/3$ unit cell (= 1.4 $cm^3\ mol^{-1}$ of $CsCuCl_3$) or about 1.8%. No further phase transitions were detected at pressures up to 6.5 GPa.

4. Discussion

We have observed a phase transition in $CsCuCl_3$ at high pressures by single-crystal diffraction, powder diffraction and Raman spectroscopy. The powder-diffraction spectra for both low- and high-pressure phases could be indexed on the same hexagonal sub-cell.

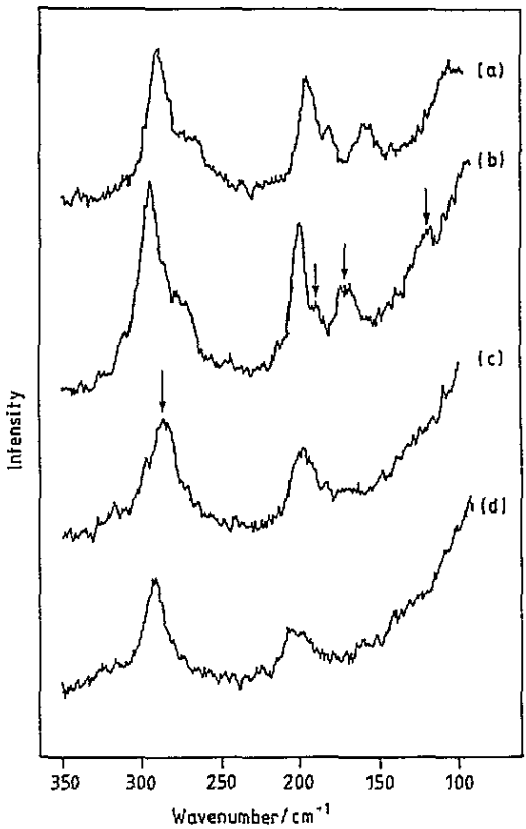

Figure 4. Pressure evolution of the Raman spectra from the low- and high-pressure phases of $CsCuCl_3$: (a) 0.07 GPa, (b) 1.59 GPa, (c) 2.01 GPa, (d) 2.91 GPa. note the disappearance of the peaks arrowed in (b) at higher pressure, and the replacement of the two peaks near 290 cm^{-1} by a single peak, arrowed in (c).

The observation of a significant discontinuity in the sub-cell volume indicates that the transition is first order in character, a conclusion supported by the co-existence of the two phases over a pressure interval in the Raman experiment. The loss of Raman lines and the disappearance from the single-crystal diffraction pattern of peaks with $l \neq 3n$ indicate that the transition is accompanied by a threefold reduction in the c-lattice repeat, and must therefore be first order (Birman 1966).

The non-symmetry-breaking lattice strains of the low-pressure phase can, in principle, couple to Q^2 and Q^3, where Q is the order parameter. Since $CsCuCl_3$ is an extremely soft material this coupling may be expected to be strong, implying that the exact relationship between Q and the free energy will be extremely sensitive to the presence of defects, including surfaces. We therefore believe that the different transition pressures that we observe in our three types of experiment arise from different densities of defects and different grain sizes, induced by the grinding of material to produce powders for the x-ray powder-diffraction and Raman experiments. The same phenomenon has been demonstrated to occur in PbO (Adams *et al* 1992).

The question remains as to the symmetry of the high-pressure phase. As we have noted, the Raman frequencies of the high-pressure phase extrapolated back to room pressure (figure 5; table 7) are similar to those of the HT $P6_3/mmc$ phase, and the c-lattice periodicity

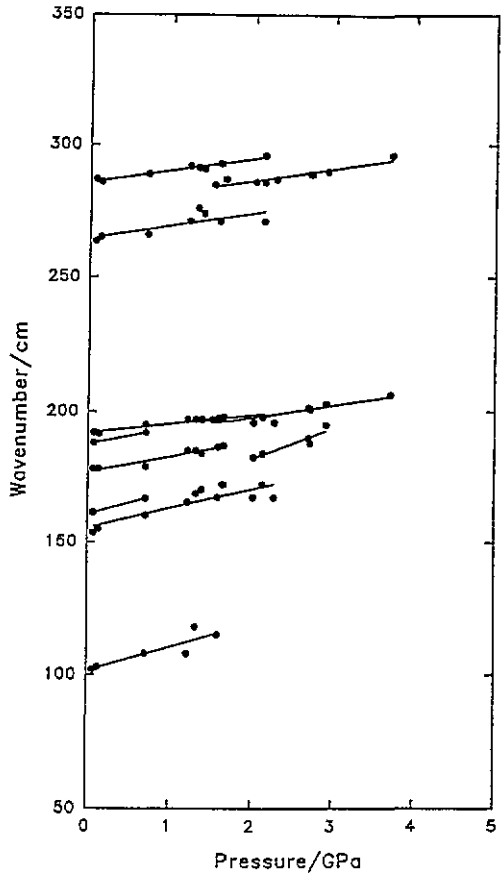

Figure 5. The variation of the Raman frequencies of $CsCuCl_3$ with pressure.

also reverts to that of the HT phase. However, it is quite possible that the true symmetry of the high-pressure phase is a *zellengleich* sub-group of $P6_3/mmc$ and that the consequent splitting of both Raman lines and x-ray diffraction peaks is sufficiently small not to be resolved in our experiments, but could be the cause of the broadening of the diffraction peaks. In either case we expect the structure of the high-pressure phase to be a statically disordered version of the dynamically disordered HT structure, with significantly different thermodynamic properties from the dynamically disordered HT phase.

The form of the phase diagram for $CsCuCl_3$ may be deduced from our measurements together with data in the literature. If the unmeasured entropy change of the high-pressure transition is assumed to arise solely from configurational disorder of long Cl–Cu–Cl bonds, i.e. $-R(\frac{1}{3}\ln\frac{1}{3} + \frac{2}{3}\ln\frac{2}{3}) = 5.3$ J mol^{-1} K^{-1}, then $\delta P/\delta T = \Delta S/\Delta V = -0.004$ GPa K^{-1}, indicating that the equilibrium phase boundary is almost flat in P–T space (figure 6). It extrapolates to ~800 K at atmospheric pressure for powder samples and ~1050 K for single crystals, temperatures far in excess of the observed transformation temperature at room pressure of 423 K (Kroese *et al* 1971). In addition, according to Hirotsu (1975) the HT phase is 0.15% greater in volume than the low-temperature phase at 423 K and 1 bar (the c-axis expands by 0.75%, the a-axis contracts by 0.3%). The enthalpy change reported by Kroese *et al* (1971), 1 cal g^{-1} = 1275 J mol^{-1}, gives a ΔS of 3 J mol^{-1} K^{-1}, implying that the slope of the equilibrium line is near isothermal and slightly positive at low pressure.

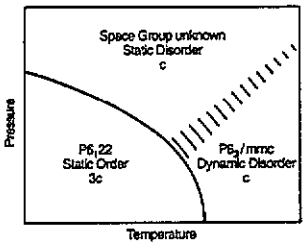

Figure 6. A possible topology for the P–T phase diagram of $CsCuCl_3$, based in part on the analogy of its behaviour with that of $CaAl_2Si_2O_8$. The high-pressure and high-temperature phases are expected to be separated by a 'diffuse' transition involving the suppression of the dynamic disorder of the Jahn–Teller distortions present in the high-temperature phase.

We therefore propose the general phase diagram topology illustrated in figure 6, in which the dynamically disordered, Jahn–Teller distorted, HT phase is separated from a statically disordered, Jahn–Teller distorted, high-pressure phase by a diffuse boundary. A similar phase diagram topology has been well characterized in $CaAl_2Si_2O_8$, where the dynamically (spatially) disordered Ca in the HT phase becomes localized in a high-pressure phase with the same space-group symmetry (Hackwell and Angel 1993).

References

Adams D M, Christy A G, Haines J and Clark S M 1992 *Phys. Rev.* B **46** 11 358–67
Akiyama K, Morioka Y and Nakagawa I 1979 *Bull. Chem. Soc. Japan* **52** 1015–8
Angel R J, Ross N L, Wood I G and Woods P A 1992 *Phase Transitions* **39** 13–32
Birman J L 1966 *Phys. Rev. Lett.* **17** 1216–9
Finger L W and Prince E 1975 *A System of Fortran IV Computer Programs for Crystal Structure Computations (NBS Technical Note 954)* (Gaithersburg, MD: NBS)
Graf H A, Shirane G, Schotte U, Dachs H, Pyka N and Iizumi M 1989 *J. Phys.: Condens. Matter* **1** 3743–63
Graf H A, Tanaka H, Dachs H, Pyka N, Schotte U and Shirane G 1986 *Solid State Commun.* **57** 369–72
Hackwell T P and Angel R J 1993 *Terra Abs.* **5** 490
Hirotsu S 1975 *J. Phys. C: Solid State Phys.* **8** L12–6
—— 1977 *J. Phys. C: Solid State Phys.* **10** 967–85
International Tables for X-ray Crystallography 1992 vol C, ed A J C Wilson (Dordrecht: Kluwer)
King H E and Finger L W 1979 *J. Appl. Crystallogr.* **12** 374–8
Koster G F, Dimmock J O, Wheeler R G and Statz H 1963 *Properties of the Thirty-two Point Groups* (Cambridge, MA: MIT Press)
Kovalev O V 1964 *Irreducible Representations of the Space Groups* (New York: Gordon and Breach)
Kroese C J and Maaskant W J A 1974 *Chem. Phys.* **5** 224–33
Kroese C J, Tindemanns-van Eyndhoven J C M and Maaskant W J A 1971 *Solid State Commun.* **9** 1707
Léger J M, Redon A M, Andraud C and Pelle F 1990 *Phys. Rev.* B **41** 9276–82
Longo J M and Kafalas J A 1971 *Solid State Chem.* **3** 429–33
Mao H-K, Xu J and Bell P M 1986 *J. Geophys. Res.* **91** 4673–6
McPherson G L and Chang J R 1973 *Inorg. Chem.* **12** 1196–9
Petzelt J, Gregora I, Vorlicek V, Fousek J, Brezina B, Kozlov G V and Volkov A A 1981 *J. Raman Spectrosc.* **10** 187–93
Ramsdell L S 1947 *Am. Mineral.* **32** 64–82
Robinson K, Gibbs G V and Ribbe P H 1971 *Science* **172** 567–70
Schlueter A W, Jacobson R A and Rundle R E 1965 *Inorg. Chem.* **5** 277–80
Tanaka H, Dachs H, Iio K and Nagata K 1986a *J. Phys. C: Solid State Phys.* **19** 4861–78
—— 1986b *J. Phys. C: Solid State Phys.* **19** 4879–96
Wells A F 1947 *J. Chem. Soc.* **69** 1662